

Article

# Spectral Shift Amplification and Polarization-Controlled Spectral Shift with Silver Metal

Pin Han \* and Yung-Chieh Tseng

Received: 1 October 2015; Accepted: 22 December 2015; Published: 26 December 2015

Academic Editor: Rita Khanna

Graduate Institute of Precision Engineering, National Chung Hsing University, 250 Kuo Kuang Road, Taichung 402, Taiwan; smart0226@gmail.com

\* Correspondence: pin@dragon.nchu.edu.tw; Tel.: +886-4-22850405; Fax: +886-4-22858362

**Abstract:** The spectral shift amplification effect and polarization-controlled spectral shifts are studied using silver (Ag) metal. The spectral shift amplification factor can be doubled by using silver compared with using water. The solid Ag metal surface also provides orientation freedom for polarization-controlled spectral shifts, benefiting data transmission applications in any direction. The liquid water interface provides only limited direction at the Brewster angle. Besides those advantages, the higher reflectivity of Ag reflects higher spectral intensity, which makes the signal easier to detect. The spectral switch phenomenon that depends on the central wavelength variation is also presented.

**Keywords:** spectral shift; shift amplification; polarization-controlled; spectral switch; silver metal

## 1. Introduction

Spectral modulation studies spectra modifications using different mechanisms, for example, optical vortex [1], aperture diffraction [2], surface plasmon [3], scattering [4], and nonlinearity [5]. Some interesting phenomena have been found, such as phase singularities [6], spectral switches [7], Talbot spectra [8]. Some applications have been suggested, such as lattice spectroscopy [9] and spatial-coherence spectroscopy [10]. Another new effect called the spectral shift amplification with water has been proposed by the author [11]. We showed that, at inclined incidence, the blue/red shifts can be controlled by the polarization selection [12]. However, there are some drawbacks in using liquid water. First the reflectance is low, making the reflected wave not easy to detect. Second the liquid water interface is always horizontal, making other orientations difficult and thus limiting its utilization. In this work, silver metal is selected to overcome these drawbacks and the spectral shift amplification effect is even more notable compared with that using water.

## 2. Theory and Numerical Results

As mentioned in the introduction, it is known that, at normal incidence, we have spectral shift amplification at oblique incidence. We also observe a spectral shift with polarization selection. Each of these two effects is investigated below.

### 2.1. Spectral Shift Amplification

The spectral shift amplification (SSA) effect occurs when a spatially coherent polychromatic radiation field is normally incident to an air-water interface and its central wavelength is varied. The reflected spectrum has larger amount of spectral shift variation than that of the incident one. The amplification factor is about 3. This effect is due mainly to a dip in the water reflectance in the

infrared region (2–4  $\mu\text{m}$ ), as shown in the circle in Figure 1a. The refractive index  $n$  and extinction coefficient  $k$  of water varies dramatically, as found in Figure 1b,c, because of the resonant interband transition at about 3.0  $\mu\text{m}$ . As mentioned above, the two main problems involved in using water are the low reflectance (only 0.7% at the dip) and the horizon interface with liquid water. Solid metals are considered in this work to improve this situation. Figure 2 illustrates the reflectance of three metals (aluminum (Al), silver (Ag), and gold (Au)) in the UV-VIS-NIR region [13]. It was found that only Ag has a sharp dip at the ultraviolet region (0.2–0.4  $\mu\text{m}$ ), as indicated by the circle. Figure 3 shows the reflectance and  $n, k$  for Ag in that region. From Figure 3a the reflectance of Ag has two minima at 0.32  $\mu\text{m}$  and 0.24  $\mu\text{m}$  respectively, as indicated by the arrows in the figure. The first minimum is the primary one because it has a much sharper dip than the second, which benefits larger SSA effect, as will be shown later. The reflectance value at the first dip is 7.2%, which is about 10 times larger than that of water. The intensity of the reflected wave can therefore be enhanced substantially.

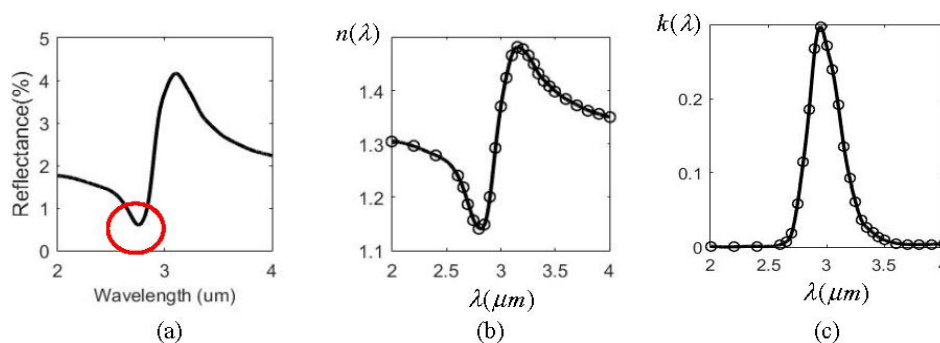


**Figure 1.** (a) Water reflectance in the infrared region (2–4  $\mu\text{m}$ ); (b) The refractive index  $n$  of water *versus* wavelength; (c) The extinction coefficient  $k$  of water *versus* wavelength.

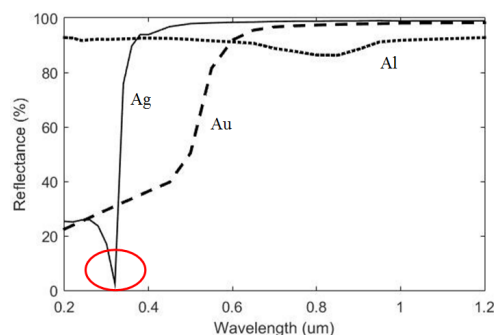


**Figure 2.** The reflectance of three metals silver (Ag) (solid line), aluminum (Al) (dotted line), and gold (Au) (dashed line) in the UV-VIS-NIR region [13].

It is well known that the optical properties of metal in the infrared regime can be best described by the Drude-Sommerfeld model [14], which basically treats the free electron effect in metals as free-electron gas, like plasma. It usually gives rise to a large negative dielectric constant value ( $\epsilon$ ) in real part and thus a strong imaginary part of the refractive index ( $n = \sqrt{\epsilon}$ ), which is just the extinction coefficient  $k$ . The consequence of this behavior is the fact that light can penetrate a metal only to a very small extent and metals have high reflectivity. However, when the visible and NUV range are considered, the response of bound electrons should be included to supplement the Drude model. This is because higher energy photons can promote the valence band electrons to the conduction band and this transition may be described by exciting oscillation in the bound electrons. There are resonant frequencies associated with the bound electrons and it can be thought of as a classical forced oscillator when they interact with the light. Consequently, the plasmon resonance mechanism [15] is needed to illustrate the optical properties of metal in the visible and NUV band, which include both free and

bound electrons' response to light. From Figures 2 and 3 it is obvious that there is a plasmon resonance for Ag around 300 nm, causing a sharp dip in reflectivity and its dispersion behavior in  $n$  and  $k$  shows the typical resonant absorption shape. The anomalous dispersion around the resonance can be utilized to create the SSA, as shown below.

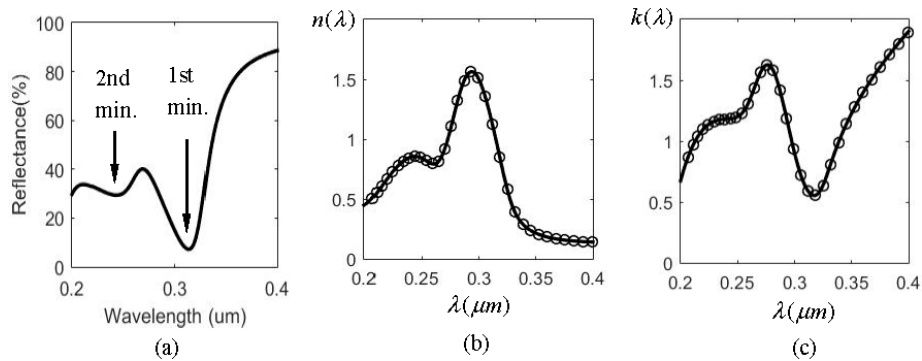


**Figure 3.** (a) Ag reflectance in the ultraviolet region (0.2–0.4  $\mu\text{m}$ ); (b) The refraction index  $n$  of Ag versus wavelength; (c) The extinction coefficient  $k$  of Ag versus wavelength [16].

The higher reflectance of Ag is mainly contributed by the free electrons in metal, while only bound charges exist in pure dielectrics like water. The free electrons result in higher extinction coefficient, as found in comparing Figure 3c with Figure 1c. Another advantage is that the free orientation usage can be obtained as well because of the solid interface. Now let us study the SSA in the Ag case. Assume the incident wave has the following Gaussian spectrum distribution

$$I^{(i)}(\lambda) = I_0 \exp \left[ - \left( \frac{\lambda - \lambda_c}{\Gamma} \right)^2 \right] \quad (1)$$

where the superscript ( $i$ ) (or ( $r$ )) denotes the incident (or reflected) light wave respectively,  $I_0$  the intensity magnitude,  $\lambda_c$  the center wavelength, and  $\Gamma$  the bandwidth. It is normally incident on an air-Ag interface, as depicted in Figure 4; consequently the reflected spectrum is modified by the reflectivity of the Ag as shown later.

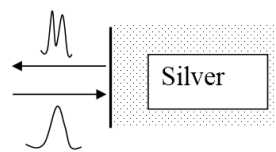


**Figure 4.** Schematic diagram for a Gaussian polychromatic wave incident on an air-silver interface and its modified reflected spectral distribution.

The reflected spectrum  $I^{(r)}(\lambda)$  is

$$I^{(r)}(\lambda) = I^{(i)}(\lambda) \times R(\lambda) \quad (2)$$

where  $R(\lambda)$  is the reflectance of the air-Ag interface as in Figure 3a. To obtain  $R(\lambda)$ , the reflection coefficient  $r(\lambda)$  by the Fresnel equation is calculated first as

$$r(\lambda) = \frac{N_{\text{air}} - N_{\text{Ag}}(\lambda)}{N_{\text{air}} + N_{\text{Ag}}(\lambda)} \quad (3)$$

where  $N_{\text{air}}$  is the refraction index of air and is set to 1.0 without loss of generality,  $N_{\text{Ag}}(\lambda) = n(\lambda) - ik(\lambda)$  is the complex refraction index of Ag and the real refraction index  $n(\lambda)$  and extinction coefficient  $k(\lambda)$

of Ag are plotted in Figure 3b,c. There the data marked with circles in the figure are experimental values [16] and they are interpolated using the cubic spline to give the curves. Once  $r(\lambda)$  is found, the reflectance  $R(\lambda) = r(\lambda) \times r(\lambda)^*$  can be obtained, where  $r(\lambda)^*$  is the complex conjugate of  $r(\lambda)$ . Figure 5a–c show the normalized spectrum of  $I^{(i)}(\lambda)$  (dotted line),  $I^{(r)}(\lambda)$  (solid line), and  $R(\lambda)$  (dashed line) for three incremental  $\lambda_c$  with  $\Gamma = 20$  nm; the value of  $\lambda_c$  is 0.307, 0.310, and 0.312  $\mu\text{m}$  in Figure 5a–c respectively. In Figure 5a,  $I^{(r)}(\lambda)$  is modified into two peaks and the left one dominates; the peak of  $I^{(r)}(\lambda)$  is blue-shifted from  $I^{(i)}(\lambda)$ , as indicated by the arrow on the top of the figure. In Figure 5b the two peaks reach the same height. In Figure 5c the right peak becomes the main peak and now the spectrum is red-shifted. Note that the amount of red-shift is larger than the blue-shift because of the slope of  $R(\lambda)$  in the right side of the dip minimum is steeper than that in the left side. The phenomenon shown in Figure 5a–c is the famous spectral switch [3,7] because there is a discontinuous jump in the spectral shift along with the variation in incident center wavelength. If we combine Figure 5a,c to produce Figure 5d, it is obvious that the shift in  $\lambda_c$  to  $I^{(i)}(\lambda)$  (dashed arrow above) is amplified into the shift in  $I^{(r)}(\lambda)$  maximum (solid arrow above). The amplification factor is 6.5 with Ag, which is more than twice that with water. Thus, both the reflected spectrum intensity (due to the higher reflectivity) and the amplification factor have increased, compared with the situation with water [11]. Note that the second minimum can also be used to generate SSA. The reflectivity at the secondary minimum ( $R = 30\%$ ) is higher than that of the first minimum (7.2%), benefiting the reflected wave. However, its shape is much shallower than the first one, thus the incident polychromatic light needs to have greater wavelength band width to utilize it. Using similar practice to plot Figure 5d in using the first minimum, Figure 6 illustrates the SSA for the second minimum with band width  $\Gamma = 20$  nm and the central wavelength  $\lambda_c$  varying from 0.22 to 0.25  $\mu\text{m}$ . The amount of maximum shift is 0.054 and thus the amplification factor is only 1.8, which is even less than that of water. Thus the first minimum is recommended for use to achieve better SSA effect.

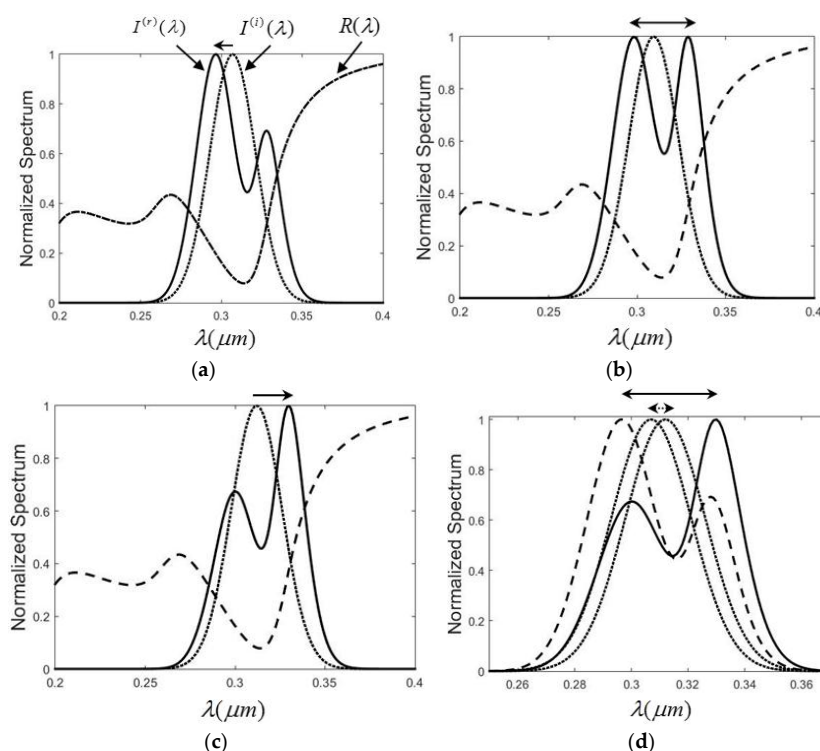


**Figure 5.** The normalized spectrum of  $I^{(i)}(\lambda)$  (dotted line),  $I^{(r)}(\lambda)$  (solid line), and  $R(\lambda)$  (dashed line) for three incremental  $\lambda_c$ . (a)  $\lambda_c = 0.307$   $\mu\text{m}$ ; (b)  $\lambda_c = 0.310$   $\mu\text{m}$ ; (c)  $\lambda_c = 0.312$   $\mu\text{m}$ . The shift of the spectrum maximum is indicated by the arrows on the top of the figure; (d) The spectral shift amplification (SSA) effect with Ag. The SSA factor is 6.5.

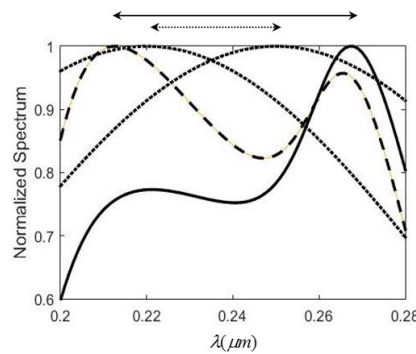


**Figure 6.** The spectral shift amplification (SSA) effect with the second minimum with band width  $\Gamma = 100$  nm and the two central wavelengths  $\lambda_c$  are 0.22  $\mu\text{m}$  and 0.25  $\mu\text{m}$ . The SSA factor is 1.8.

## 2.2. Polarization-Controlled Spectral Shift

It is well known that when the incidence angle is not zero, the interface reflectance varies for different polarizations. The reflection coefficient is modified, according to the Fresnel equations, as

$$\begin{aligned} r_s(\lambda) &= \frac{N_{air}\cos(\theta_1) - N_{Ag}(\lambda)\cos(\theta_2)}{N_{air}\cos(\theta_1) + N_{Ag}(\lambda)\cos(\theta_2)} \\ r_p(\lambda) &= \frac{N_{air}\cos(\theta_2) - N_{Ag}(\lambda)\cos(\theta_1)}{N_{air}\cos(\theta_2) + N_{Ag}(\lambda)\cos(\theta_1)} \end{aligned} \quad (4)$$

where  $\theta_1$  and  $\theta_2$  are the incidence and refraction angles respectively and the polarization states are indicated by the subscripts  $s$  (TE) and  $p$  (TM). Note that  $N_{Ag}(\lambda)$  is complex, so is  $\cos(\theta_2)$ . The correct way to get it is, for a given  $\theta_1$ , using Snell's Law ( $N_{air}\sin(\theta_1) = N_{Ag}(\lambda)\sin(\theta_2)$ ) to give the complex  $\sin(\theta_2)$  and using the triangular equity  $\cos(\theta_2) = [1 - \sin^2(\theta_2)]^{1/2}$  to obtain  $\cos(\theta_2)$ . The reflected spectral intensities for the two polarizations are

$$I_{s,p}^{(r)}(\lambda) = E_{s,p}^{(r)}(\lambda) \times [E_{s,p}^{(r)}(\lambda)]^* = I^{(i)}(\lambda) \times R_{s,p}(\lambda) \quad (5)$$

where  $R_{s,p}(\lambda) = r_{s,p}(\lambda) \times r_{s,p}(\lambda)^*$  is the reflectance for the  $s$  and  $p$  polarizations, as shown in Equation (4). From the previous work [12] and the Fresnel equations, it is known that the largest difference between  $R_s(\lambda)$  and  $R_p(\lambda)$  exists at the Brewster angle ( $\theta_B$ ), being about  $50^\circ$  at  $\lambda = 2.7$   $\mu\text{m}$  for water, as shown in Figure 7a in log scale. For metals, the angle with minimum  $R_p(\lambda)$  is called the principle angle of incidence or the quasi-Brewster angle  $\theta_{B'}$  [17]. Figure 7b shows the  $R_s(\lambda)$  and  $R_p(\lambda)$  for aluminum at  $\theta_{B'} = 60^\circ$  at  $\lambda = 0.3$   $\mu\text{m}$ . Comparing Figure 7b with Figure 7a, we note that both the reflectance of  $R_s(\lambda)$  and  $R_p(\lambda)$  of Ag are higher than those of water; particularly the dip region of  $R_p(\lambda)$  for Ag and water is in the order of  $10^{-1}$ – $10^{-2}$  and  $10^{-5}$ – $10^{-6}$  respectively. All of these also benefit the stronger reflected spectrum intensity, especially the p-polarization light wave. Using the reflectance in Figure 7b and setting  $\lambda_c = 0.3$   $\mu\text{m}$  with  $\Gamma = 40$  nm for  $I^{(i)}(\lambda)$ , Figure 8 illustrates the normalized spectral distributions and shifts for the two polarizations. Figure 8a shows that the maximum of the  $I_s^{(r)}(\lambda)$  is blue-shifted and it is a red-shift for  $I_p^{(r)}(\lambda)$  in Figure 8b. The number of blue and red shifts are  $-14$  and  $33$  nm respectively. We confirm that the shift in the reflected wave from Ag can also be controlled by selecting the polarization state, just like in the water case. The reflected intensity is much higher than that of water due to the high Ag reflectance. Another advantage for utilizing aluminum is the freedom of orientation, as depicted in Figure 9. As suggested in the water case, the polarization-controlled spectral shifts can be used as a digital transmission scheme. In Figure 9a the data being transmitted is shown in the first row, and we can designate the blue-shift (B) and red-shift (R) of the reflected spectrum as a bit of "1" or "0" respectively, as denoted in the second row. If these data need to be sent to a receiver located at  $\theta$  to the right of the vertical direction, as shown in Figure 9b, all we need to do is to set

the Ag surface normal to the left of the vertical at  $\theta_{B'} - \theta$ . When the light is incident on Ag with the incident angle  $\theta_{B'} = 60^\circ$ , the reflected light will head toward the receiver, due to the law of reflectivity. Thus by selecting the polarization states  $s$  (TE) or  $p$  (TM), the blue or red shift in reflected light can be controlled, as in Figure 8, and the data can be transmitted and detected, as shown in the bottom row of Figure 9a,b. However, when liquid water is used the normal of the surface is always vertical and the angle of the receiver can only be  $\theta_B = 50^\circ$ , as shown in Figure 9c, which limits its usage for data transmission.

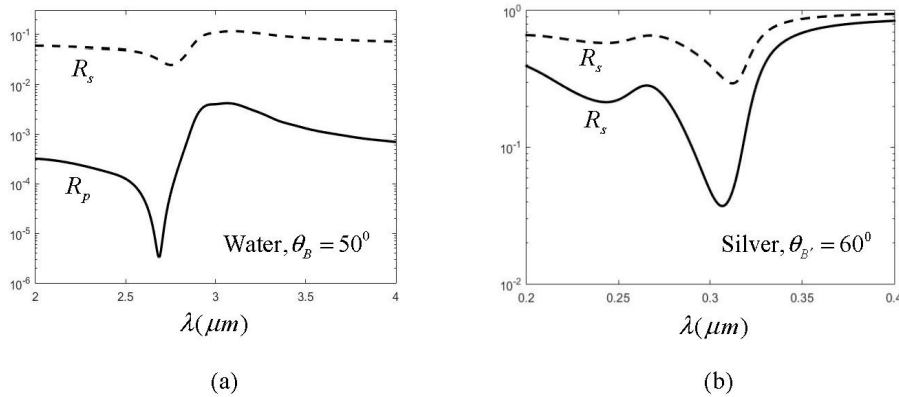


Figure 7. (a) The reflectance of  $R_s(\lambda)$  and  $R_p(\lambda)$  of water; (b) The reflectance of  $R_s(\lambda)$  and  $R_p(\lambda)$  of Ag.

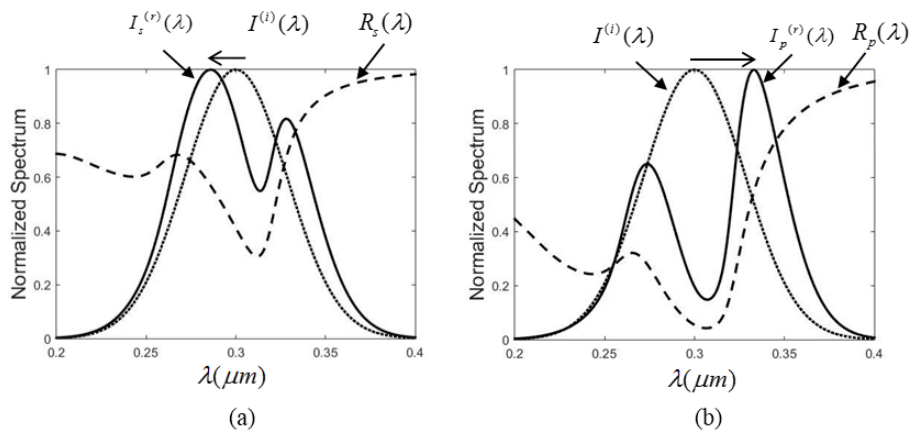
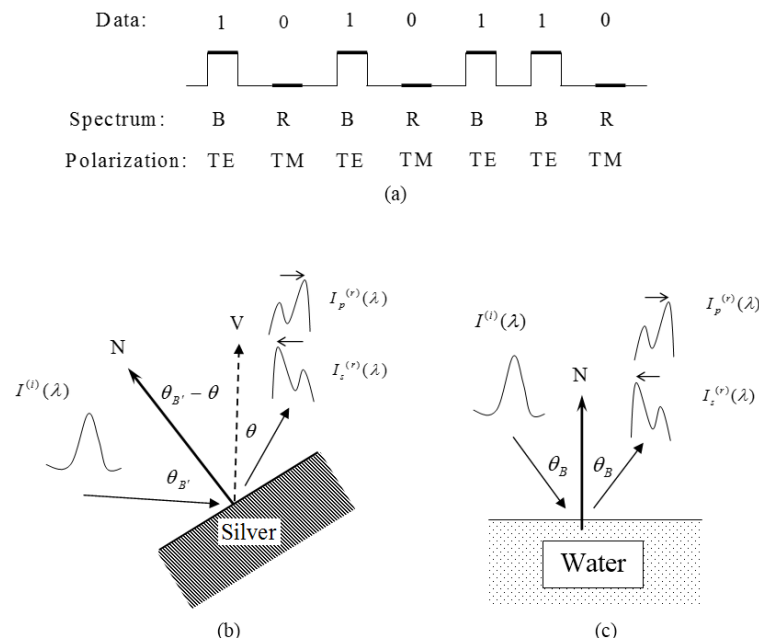


Figure 8. (a) Normalized spectrum for  $I_s^{(r)}(\lambda)$ ; (solid line),  $I^{(i)}(\lambda)$  (dotted line) and  $R_s(\lambda)$  (dashed line); (b) Normalized spectrum for  $I_p^{(r)}(\lambda)$ ; (solid line),  $I^{(i)}(\lambda)$  (dotted line) and  $R_s(\lambda)$  (dashed line). The shift of the spectrum maximum in (a) and (b) are blue-shift and red-shift respectively, as indicated by the arrows on the top of the figure.



**Figure 9.** (a) The schematics for a digital data transmission scheme with polarization control; (b) Using Ag for transmission task at arbitrary angle  $\theta$  to the right of vertical direction (V); (c) Only the direction near Brewster angle can be used for that purpose with water.

### 3. Conclusions

This work investigated the advantages of using silver metal to achieve the spectral shift amplification effect at normal incidence and polarization-controlled spectral shifts at oblique incidence. Compared with water the Ag amplification factor is twice that of water. Using solid Ag metal provides orientation freedom for spectral shifts in data transmission in any direction, while only one fixed direction at the Brewster angle is found with liquid water. The spectral switch phenomenon was also presented in detail. The greater Ag reflectivity also offers much stronger reflected spectral intensity, which is good for the receiving end.

**Acknowledgments:** This work was supported by National Chung Hsing University, Taiwan, by the Ministry of Science and Technology of Republic of China under Contract NSC 104-2221-E-005-069-MY3, Contract NSC 102-2622-E-005-013-CC3.

**Author Contributions:** Pin Han suggested the idea, wrote the paper and contributed in all activities. Yung-Chieh Tseng performed the numerical works and analyzed the results.

**Conflicts of Interest:** The authors declare no conflict of interest.

### References

- Ding, P.; Ren, H. Propagation law of partially coherent vortex beam. *Opt. Eng.* **2012**. [[CrossRef](#)]
- Han, P. Spectral anomalies for a right triangle aperture with an adjustable hypotenuse slope. *J. Opt. A Pure Appl. Opt.* **2009**. [[CrossRef](#)]
- Kanseri, B.; Kandpal, H.C.; Budhani, R.C. Far field spectrum in surface plasmon-assisted Young's double-slit interferometer. *Opt. Commun.* **2012**, *285*, 4811–4815. [[CrossRef](#)]
- Ding, C.L.; Cai, Y.J.; Zhang, Y.T.; Pan, L.Z. Scattering-induced changes in the degree of polarization of a stochastic electromagnetic plane-wave pulse. *J. Opt. Soc. Am. A* **2012**, *29*, 1078–1090. [[CrossRef](#)] [[PubMed](#)]
- Han, P. All optical spectral switches. *Opt. Lett.* **2012**, *37*, 2319–2321. [[CrossRef](#)] [[PubMed](#)]
- Soskin, M.S.; Vasnetsov, M.V. Singular optics. In *Progress in Optics*; Wolf, E., Ed.; Elsevier: Amsterdam, The Netherlands, 2001; Volume 42, p. 219.
- Pu, J.; Zhang, H.; Nemoto, S. Spectral shifts and spectral switches of partially coherent light passing through an aperture. *Opt. Commun.* **1999**, *162*, 57–63. [[CrossRef](#)]

8. Han, P. Spectra restoration of a transmissive periodic structure in near-field diffraction (Talbot spectra). *J. Opt. Soc. Am. A* **2015**, *32*, 1076–1083. [[CrossRef](#)] [[PubMed](#)]
9. Han, P. Lattice spectroscopy. *Opt. Lett.* **2009**, *34*, 1303–1305. [[CrossRef](#)] [[PubMed](#)]
10. Wolf, E.; James, D.F.V. Correlation-induced spectral changes. *Rep. Prog. Phys.* **1996**, *59*, 771–818. [[CrossRef](#)]
11. Han, P. Spectral shifts with polarization control. *J. Opt.* **2013**. [[CrossRef](#)]
12. Han, P. Spectral shift amplification. *Opt. Lett.* **2012**, *37*, 4895–4897. [[CrossRef](#)] [[PubMed](#)]
13. Lee, C.C. *Thin Film Optics and Coating Technology*, 4th ed.; Yihsient: Taipei, Taiwan, 2004; p. 145.
14. Ashcroft, N.W.; Mermin, N.D. *Solid State Physics*; Saunders College Publishing: Orlando, FL, USA, 1976; p. 2.
15. Novotny, L.; Hecht, B. *Principles of Nano-Optics*; Cambridge: New York, NY, USA, 2006; p. 378.
16. Rakić, A.D.; Djurišić, A.B.; Elazar, J.M.; Majewski, M.L. Optical properties of metallic films for vertical-cavity optoelectronic devices. *Appl. Opt.* **1998**, *37*, 5271–5283. [[CrossRef](#)] [[PubMed](#)]
17. Hecht, E. *Optics*, 4th ed.; Addison Wesley: New York, NY, USA, 2002; p. 131.



© 2015 by the authors; licensee MDPI, Basel, Switzerland. This article is an open access article distributed under the terms and conditions of the Creative Commons by Attribution (CC-BY) license (<http://creativecommons.org/licenses/by/4.0/>).